EXCESS NOISE SPECTRAL ANALYSIS OF BORON

IMPLANTED LAYERS IN SILICON

By

JAWAHAR LAL TANDON

Bachelor of Technology

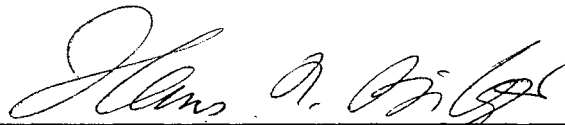Indian Institute of Technology

Kanpur, India

1970

Submitted to the Faculty of the Graduate College
of the Oklahoma State University
in partial fulfillment of the requirements
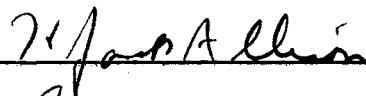for the Degree of
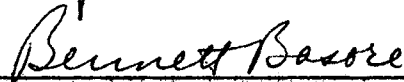MASTER OF SCIENCE
May, 1973

EXCESS NOISE SPECTRAL ANALYSIS OF BORON

IMPLANTED LAYERS IN SILICON

Thesis Approved:

_____
Thesis Adviser

_____

_____

_____
Dean of the Graduate College

ACKNOWLEDGEMENTS

TABLE OF CONTENTS

LIST OF FIGURES

CHAPTER I

INTRODUCTION

Most electronic devices possess an additional dominant kind of noise at low frequencies. This form of noise is referred to as "excess noise" or "flicker noise" or current noise or "1/f noise". For any device application involving low-level low frequency electronic signal processing, an understanding, knowledge and estimation of excess noise proves indispensable to optimize a good signal to noise ratio.

Many studies, both experimental and theoretical, have been done on excess noise in electronic devices. In general it is well established that this kind of noise has two distinct properties in contrast to Nyquist (thermal) noise in that (a) it is present only in the state of thermodynamic nonequilibrium when there is external power flow through the device, and (b) its power spectral density S_p is proportional to f^{-n} where f is the frequency and n is a positive number close to 1. Interesting features about excess noise stem from the fact that it is present in many materials and extends over a large range of frequencies; it has been found to be of 1/f type at frequencies as low as 10^{-4} Hz in carbon resistors, germanium filaments and transistors, and as high as 10^6 Hz in carbon resistors (1,2).

Theories, both physical (1,3,4,5,6) and empirical (7,8,9) have been proposed in an attempt to understand the nature and source of the excess noise. An attempt has also been made for many years to suggest

1

techniques that would reduce this kind of noise in electronic devices if not eliminate it. Considering the relatively simple physical mechanism and formulas explaining and describing the thermal noise of resistors and the shot noise of p-n junctions and transistors, it appears amazing that the excess noise still leaves many questions to be answered. Recent studies made to understand the nature of the excess noise (5,10) point out that, "The exact physical phenomenon that produces this noise is not known."

This thesis presents a study of the excess noise involving its measurement in boron-implanted layers (resistors) in silicon as a further step to understand its behavior and origin. Since the ion implantation procedure (Appendix A) provides a novel method of precision doping in which the geometry of the layer and the active carrier density can be controlled precisely (< $\pm$ 10%), the analysis of results provides not only a close examination of the dependence of the excess noise on various device parameters but also a means to investigate the validity of the various theories available up to date to explain the origin of the excess noise.

CHAPTER II

TECHNICAL DETAILS OF THE DEVICES

The devices used for investigating excess noise were ion implanted
resistors with simple geometries (box type) formed by implanting boron
ions in the energy range of 50 to 110 keV into silicon. The boron doses
used ranged from 2.5×10^{12} to 1.0×10^{14} boron ions/cm^2, resulting in
sheet resistances of 100 to 500 ohms/☐ for complete annealing. In
order to achieve somewhat larger resistances, partial annealing was em-
ployed. A detailed picture of the devices used with their nomenclature
is shown in Appendix B.

All the devices (implanted layers) were checked to possess adequate
electrical insulation to the substrate (leakage currents to the substrate
$I_{\ell} < 10^{-7}$ A were typically measured at a few volts reverse bias between
the implanted p-layer and the n-substrate). Therefore for all practical
purposes, neglecting interfacial effects, the current density in the
layer could be approximated by a one dimensional current flow.

The current-voltage (I_D vs V_D) characteristics of some of the
devices were measured to test the variation of resistance for different
biases in the current (I_D) range of interest (0 - 100 μA). The samples
chosen were devices available with the three different doses of implanta-
tion 2.5×10^{12}, 1.0×10^{13} and 1.0×10^{14} boron ions/cm^2 and all made
with the energy of implantation equal to 80 keV. Figures 1, 2, and 3
represent I_D-V_D plots of resistors R_{36} and R_{86} in devices 20, 27 and 32,
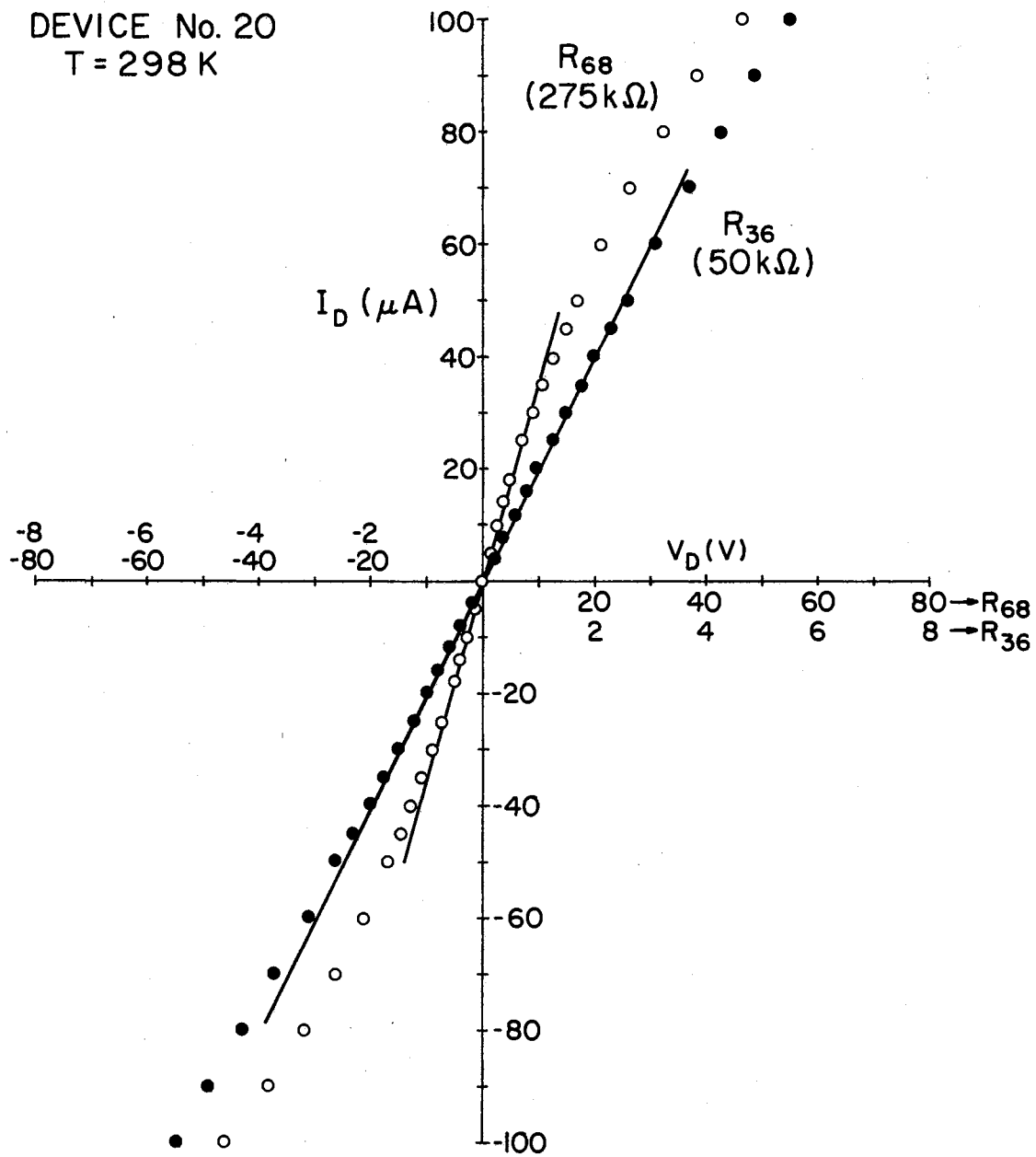
Figure 1. Current Voltage Characteristics of Resistors R_{68} and R_{36} in Device No. 20
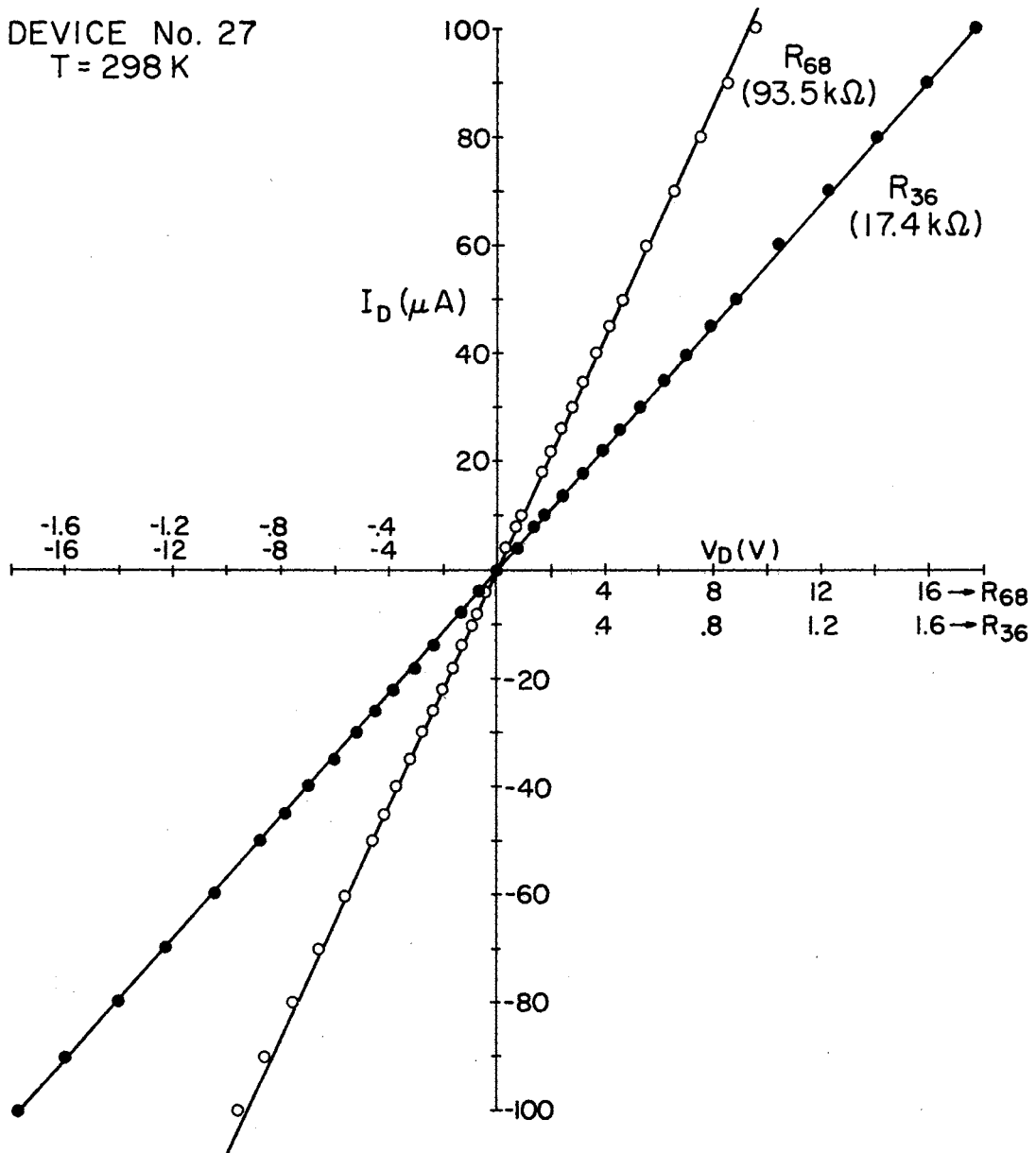
Figure 2. Current Voltage Characteristics of Resistors R_{68} and R_{36} in Device No. 27
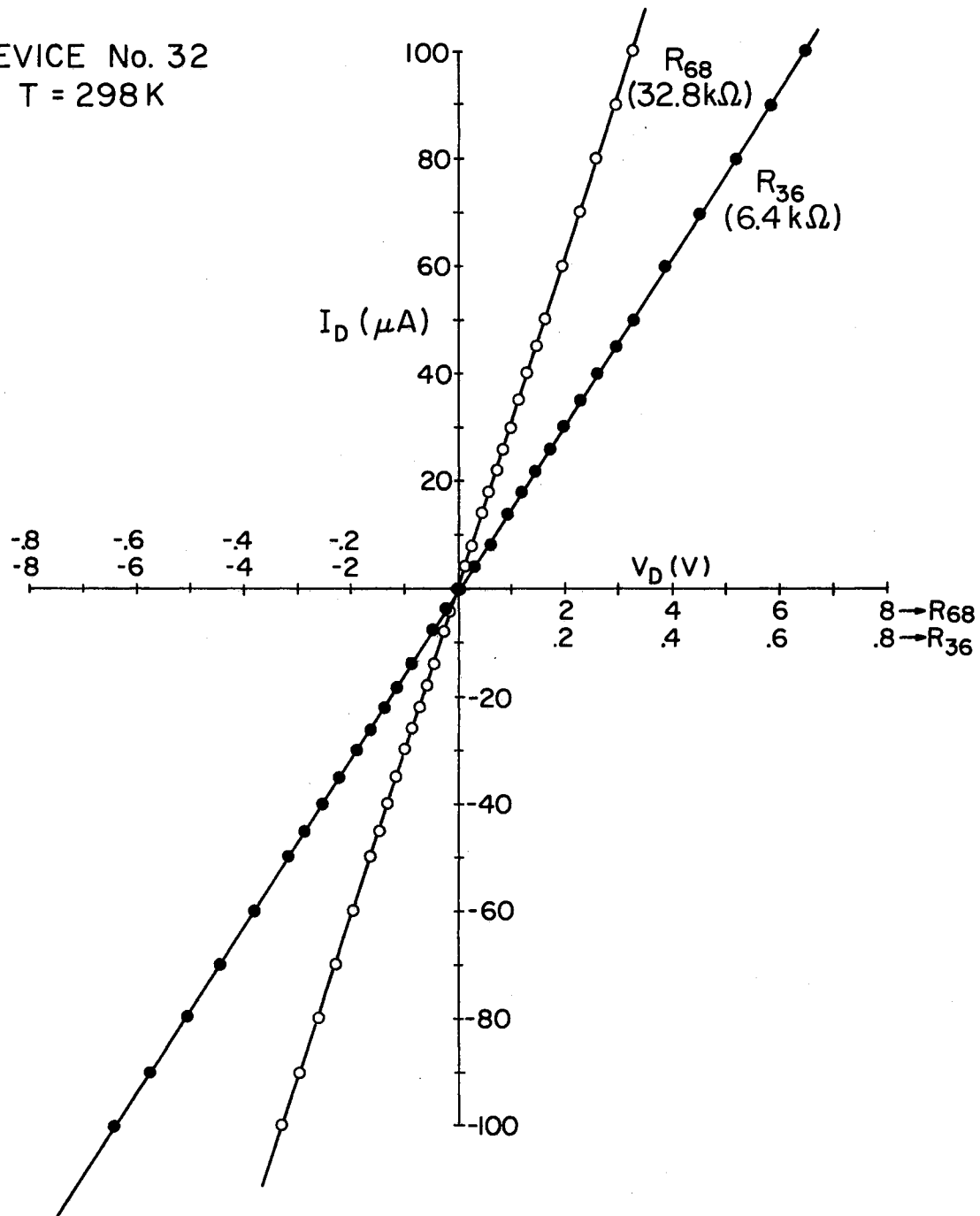
Figure 3. Current Voltage Characteristics of Resistors R_{68} and R_{36} in Device No. 32

respectively. At higher values of V_D the resistance values tend to increase, the effect being dominant in device 20 with the least doping $(2.5 \times 10^{12} B^+ \text{ ions/cm}^2)$ where high values of V_D are required to obtain the desired range of $I_D = 0 - 100 \mu A$. However, for higher doped cases, devices 27 and 32, resistors are strictly linear for the above current range. In noise measurements care was taken to use a value of V_D such that the devices operated in the linear region.

The increase of resistance for large biases across the device when used with the substrate connected to the most positive terminal, as shown in Figure 4, is due to pinching produced in the channel as a result of increasing bias between the drain and the substrate along the channel. Any effect of heating which tends to increase the number of free carriers in the channel, thereby reducing the resistance value, is probably negligible.

DEPLETION LAYER PROFILE
FOR SMALL BIAS

DEPLETION LAYER
PROFILE FOR
LARGE BIAS

+

B IMPLANTED
P LAYER

−

$n - S_i$
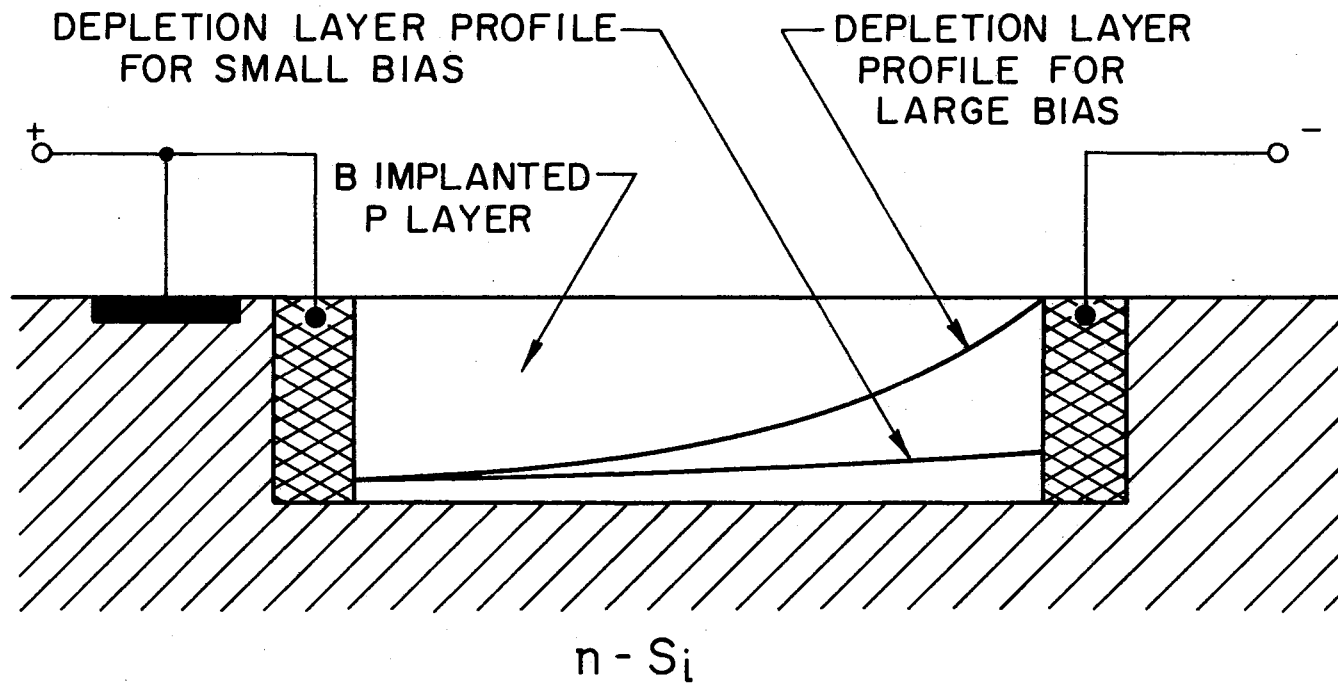
Figure 4.   Schematic Representation of Current Pinching in the Channel

CHAPTER III

EXPERIMENTAL PROCEDURES AND PRESENTATION

OF NOISE DATA

Details of the experimental set up used for noise measurement and calibration are shown in Appendix C.

The excess noise spectra of the ion implanted layers were measured in the frequency range of 10 Hz to 1 MHz. The results were presented as noise current sources $\Delta I(f)$ in parallel with the device admittance $Y(f)$ and referred to the noise current $Ieq(f)$ of a saturated vacuum diode (Figure 5).

All the spectra measured have the form

$$Ieq(f) = Ieq_\infty + (\text{constant})\ f^{-n} \qquad . \qquad (3.1)$$

The frequency independent part Ieq_∞ was in all cases quantitatively (within $\pm$ 10%) identified as the thermal noise of the device and input circuitry, i.e., (see reference 11),

$$Ieq_\infty = \frac{2kT}{q}\ Re\{Y(f)\} \qquad (3.2)$$

where

    k = Boltzmann Constant (VAS/K);

    T = absolute temperature (K); and

    $Re\{Y(f)\}$ = real part of admittance at the device electrodes.

Another characterization was used to represent only the excess noise component by defining
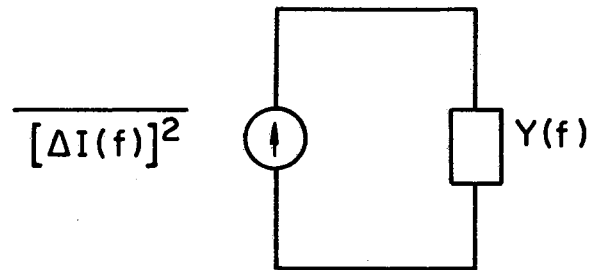
$$\overline{[\Delta I(f)]^2} = 2q\, I_{eq}(f)\,\Delta f$$

WHERE q = ELECTRON CHARGE (As)

Δf = BANDWIDTH (Hz)

Figure 5. Noise Representation of the
          Device

$$Ieq*(f) = Ieq(f) - Ieq_\infty = (constant)\ f^{-n} \qquad . \qquad (3.3)$$

It is important to note that in all the measured spectra no other forms of fundamental noise were observed; in particular there was no evidence of generation-recombination (g-r) noise.

CHAPTER IV

EXPERIMENTAL INVESTIGATIONS AND RESULTS

Noise spectra (frequency range 10 Hz - 1 MHz) of the excess noise were measured and their dependence on the following parameters were investigated:

(a) D-C current I_D through the device (range 1 μA to 100 μA);

(b) geometry and contacts (ratio of widths 1:5 with length/width ratio constant, measurements on probes along the current path - see Appendix B);

(c) temperature (room temperature, $\sim$ 300 K, to liquid nitrogen temperature, 77 K);

(d) implantation dose (2.5×10^{12} to 1.0×10^{14} B^+ ions/cm^2);

(e) implantation energy (50 keV to 110 keV); and

(f) substrate bias (0 to 10 V).

Results obtained are shown in Figures 6 through 16.

4.1 Current Dependence of the Excess Noise

Figure 6 shows the excess noise component Ieq* of R_{54} in the device 20 at a particular frequency $f = 2$ kHz vs. device current I_D. The slope of the line being equal to 2 in the current range 0 - 100 μA suggests that Ieq* strictly varies as I_D^2.
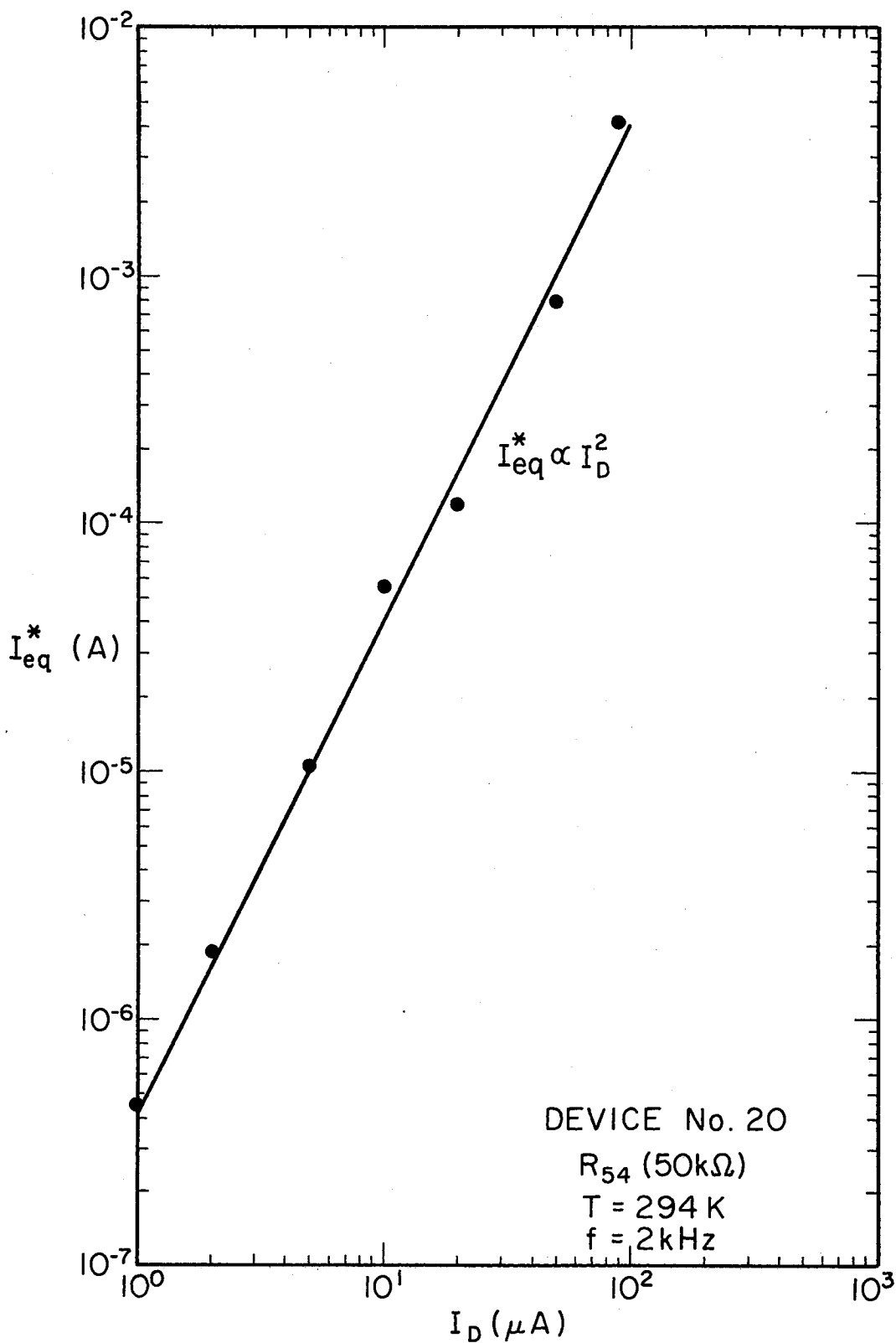
Figure 6. Excess Noise Component (Ieq*) vs. Device Current (I_D) of Resistor R_{54} in Device No. 20 at 2 kHz

4.2 Device Length Dependence of the Excess Noise

Probe measurements were made on the devices 20, 27 and 32 in order to investigate the location of the excess noise in the resistor R_{86}. The results are shown in Figures 7, 8, and 9, respectively. All of these plots lead to two important and interesting conclusions; namely (a) the excess noise is not generated at the contacts principally, for if it did, Ieq* of R_{27}, R_{17} or R_{12} (which do not involve contacts) should have been considerably smaller than Ieq* of R_{26}, R_{76}, R_{16} or R_{86} (which involve contacts), and (b) the excess noise does not vary much with the length (L) of the device (less than a factor 3 for a change of L by factor 5). A simple model of spatially uncorrelated excess noise would result in Ieq* ∞ 1/L which is found not to be true. It appears that there is a correlation between the excess noise contributions of different lengths of the channel.

4.3 Device Width Dependence of the Excess Noise
With L/W = Constant

Figures 10, 11, and 12 represent the noise spectra of resistors R_{54}, R_{43}, and R_{36} in the devices 20, 27, and 32, respectively. These resistors have different lengths (L) and widths (W) but the same L/W ratio. Since all the layers are implanted with the same energy of implantation, their depths (D) are the same. Essentially the resistors have the same values (within a few percent) for each of the devices. The plots 10 and 11 prove that although the resistors have the same thermal noise asymptote at high frequencies, their low frequency excess noises are quite different. The resistor R_{54} which is the smallest in dimensions produces the largest excess noise. A close examination suggests, that for the
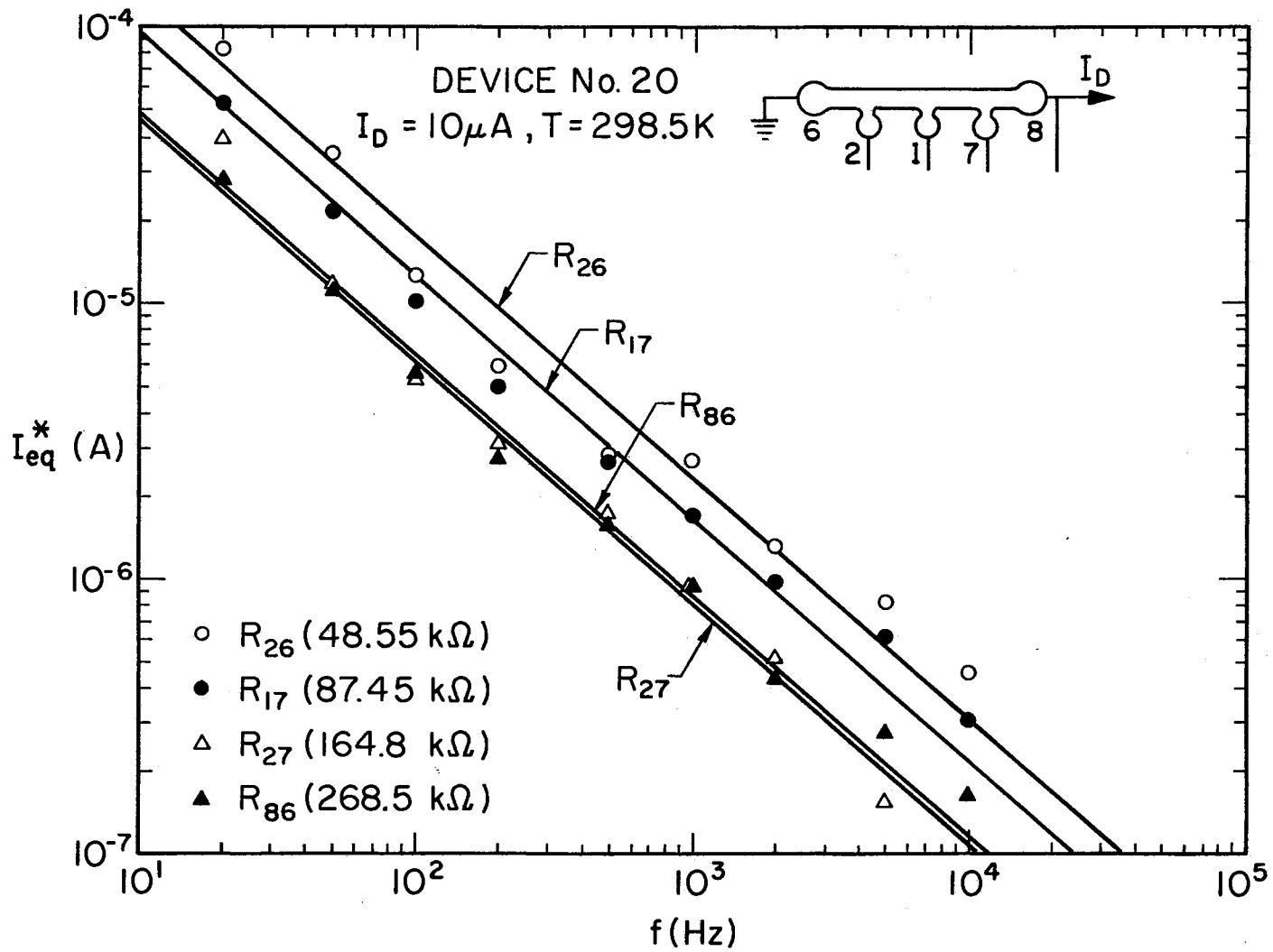
Figure 7. Excess Noise Component (Ieq*) Spectra of Resistors in Device No. 20 for I_D = 10 μA

15
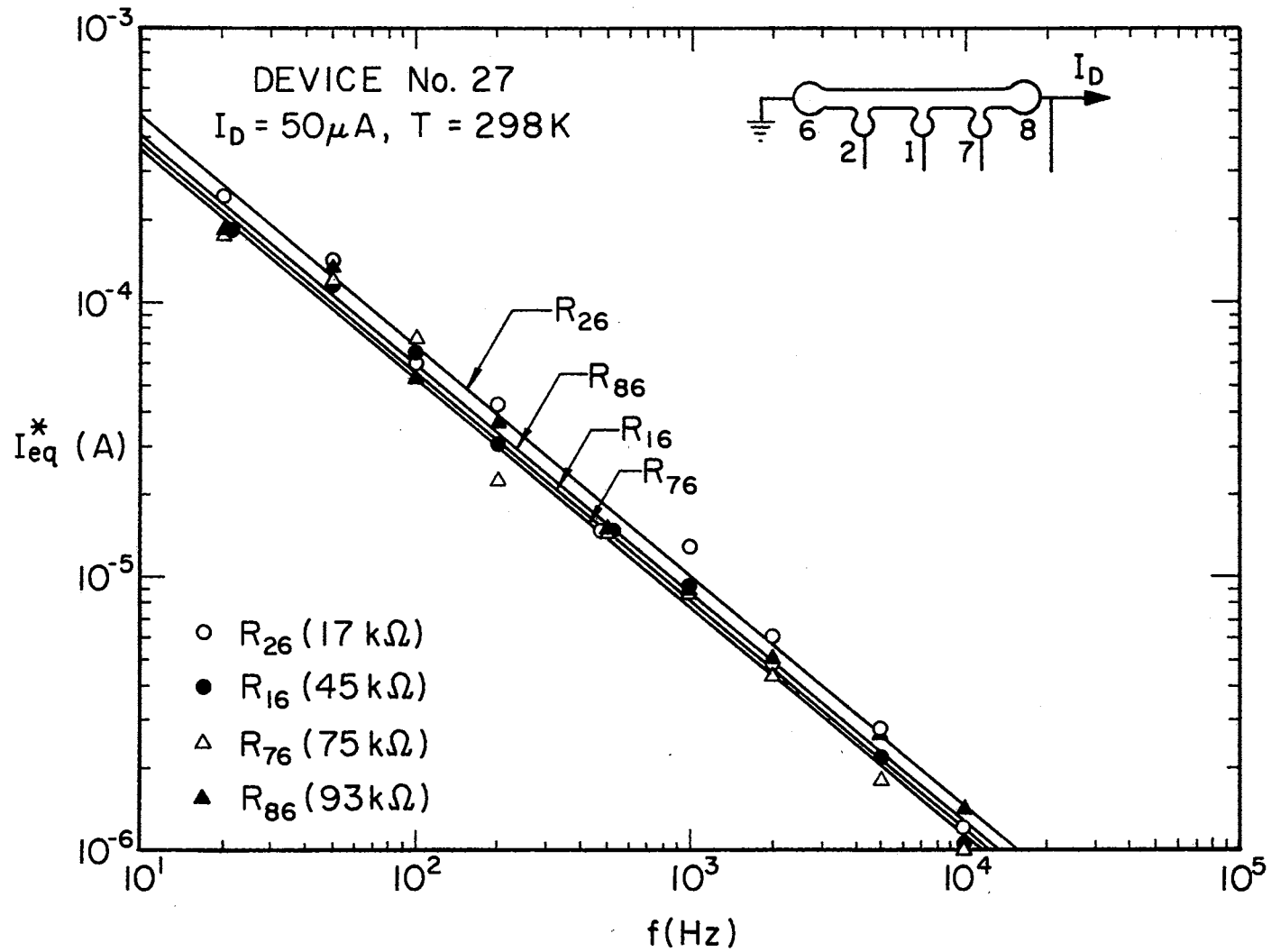
Figure 8. Excess Noise Component (Ieq*) Spectra of Resistors in
Device No. 27 for I_D = 50 µA
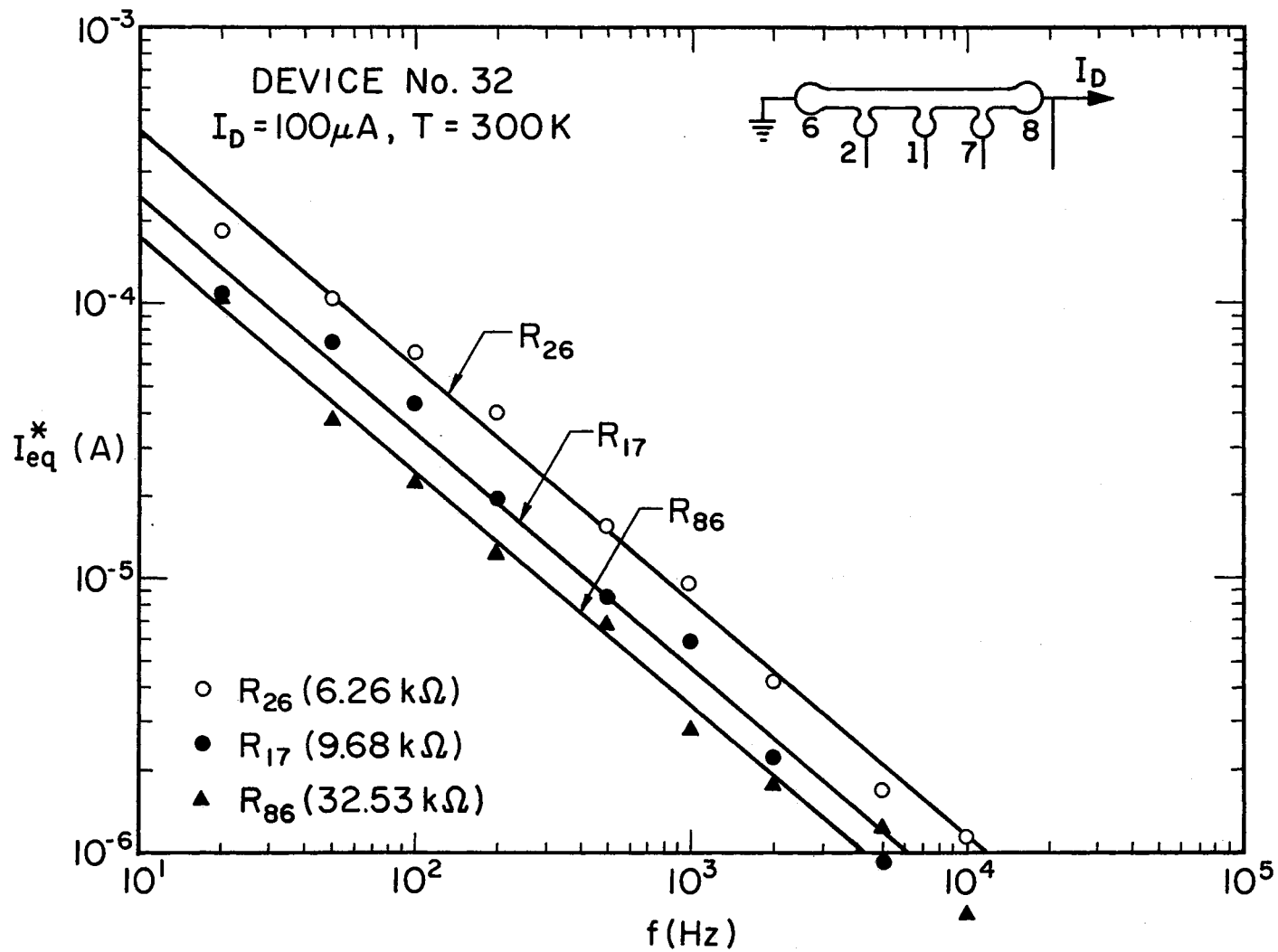
Figure 9. Excess Noise Component (Ieq*) Spectra of Resistors in
Device No. 32 for I_D = 100 µA
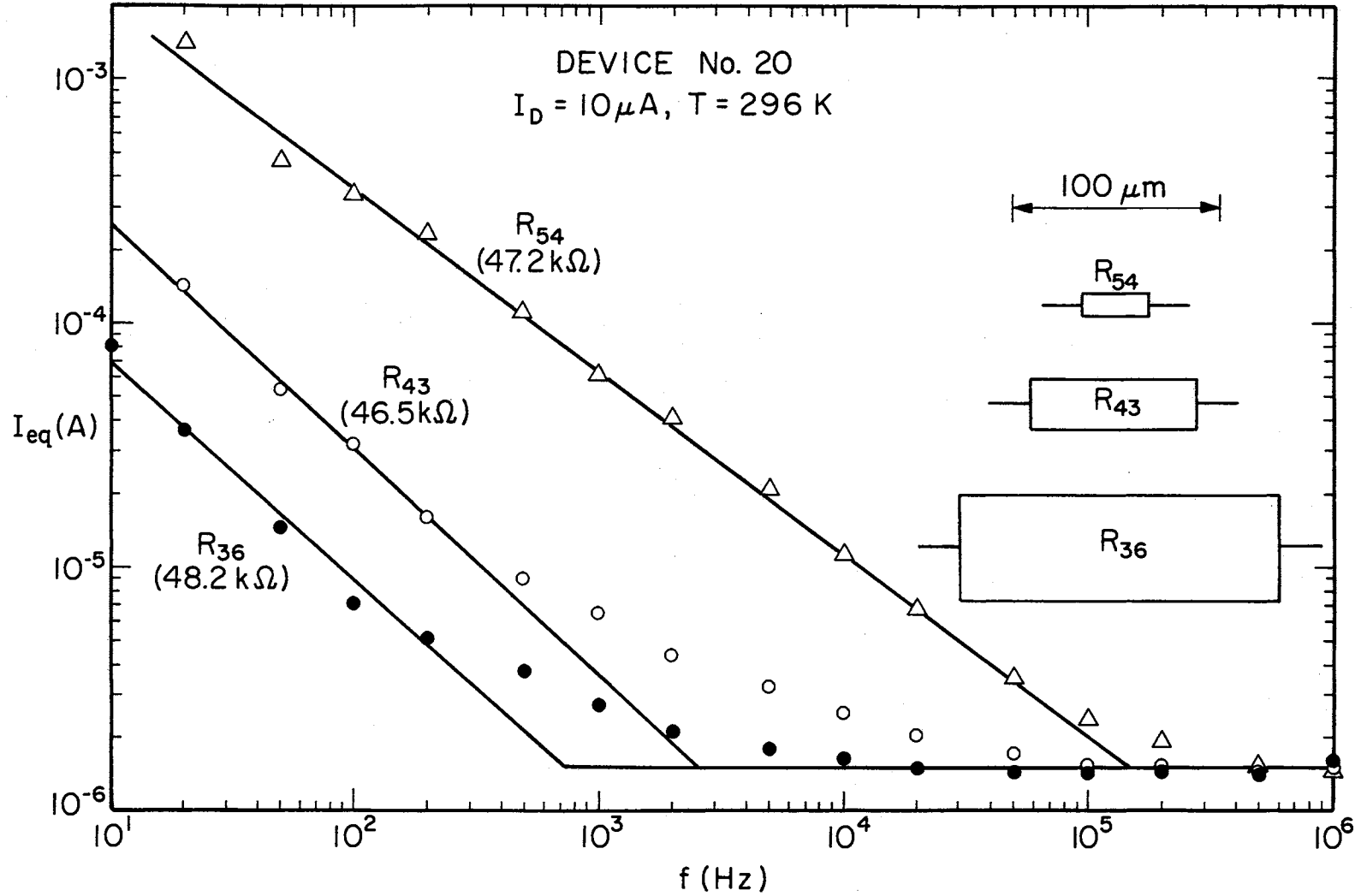
Figure 10. Noise Spectra of Resistors R_{54}, R_{43}, and R_{36} in Device No. 20 for $I_D = 10$ μA
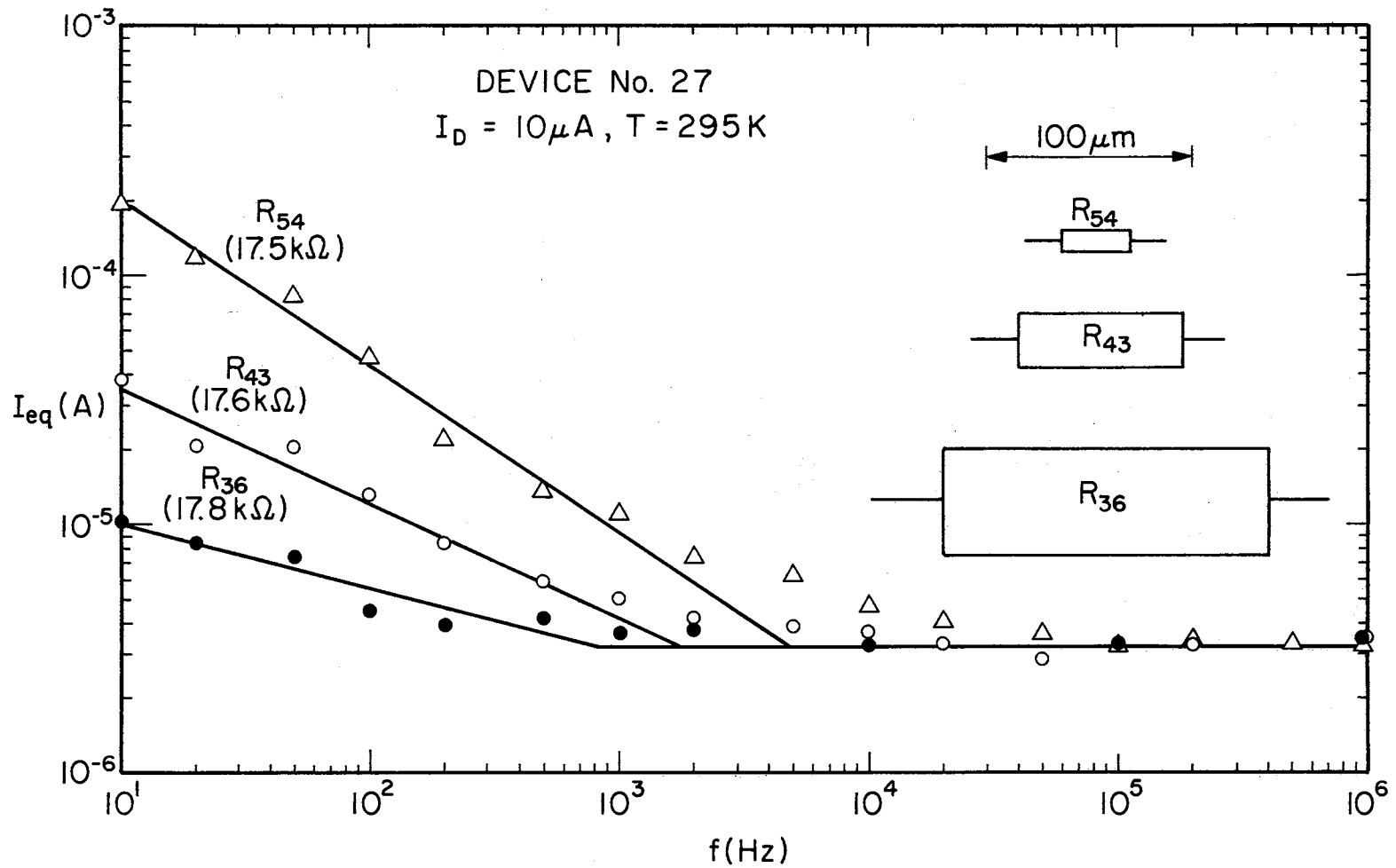
Figure 11. Noise Spectra of Resistors R_{54}, R_{43}, and R_{36} in Device No. 27 for I_D = 10 μA
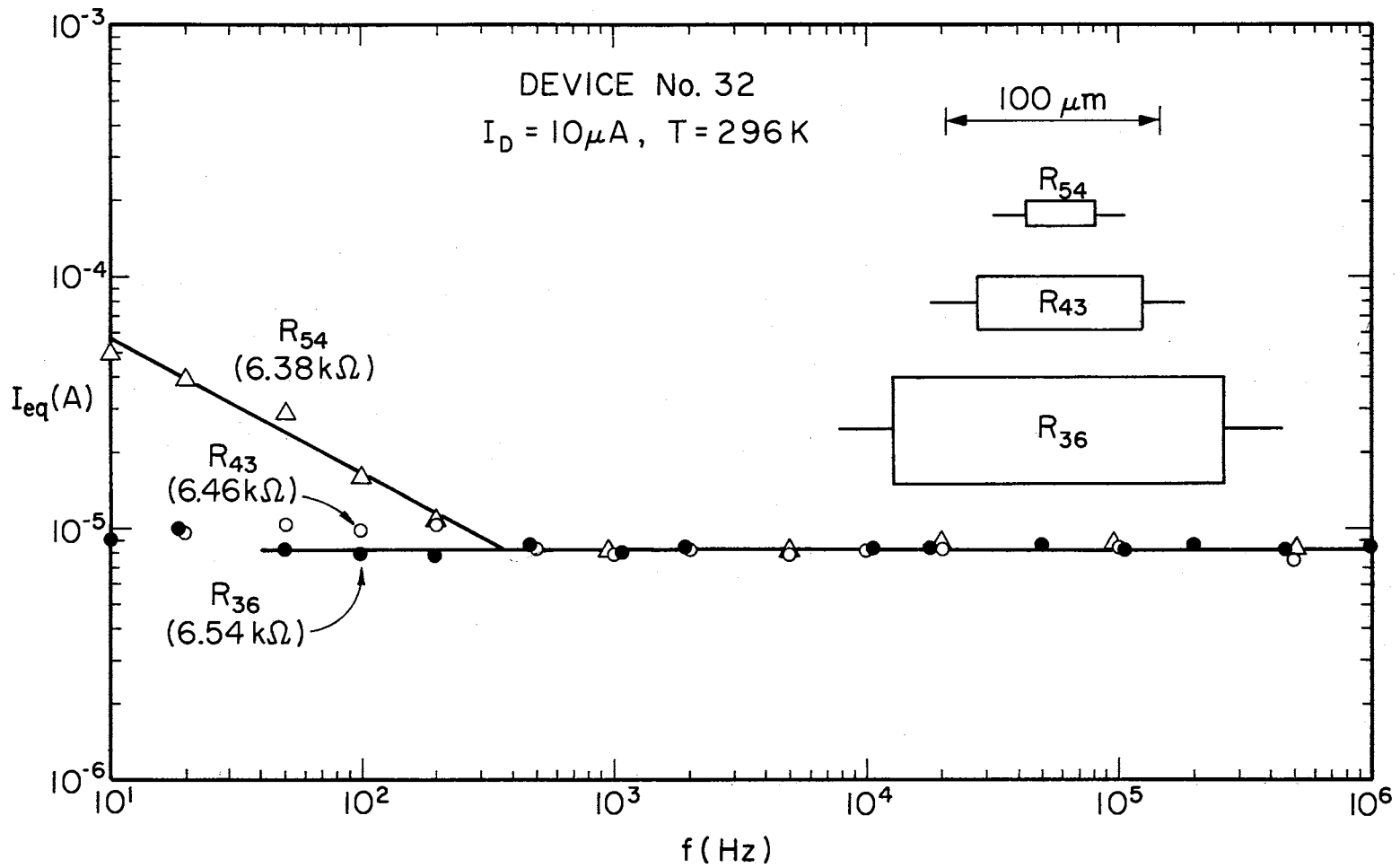
Figure 12. Noise Spectra of Resistors R_{54}, R_{43}, and R_{36} in Device No. 32 for I_D = 10 μA

resistors R_{54}, R_{43} and R_{36} which have their widths in the ratio 1:2:5, respectively, Ieq* ∞ $1/W^2$ (considering the effect of a change of L being negligible as postulated earlier). In Figure 12 which shows the noise spectra of the device 32 (highest implantation dose = 1.0 x 10^{14} B^+ ions/cm^2), only the excess noise of R_{54} appears whereas for R_{43} and R_{36} no excess noise component can be distinguished from the thermal noise component in the frequency range employed. This is explained by an inverse dependence of the excess noise on the implantation dose (to be discussed later).

4.4 Temperature Dependence of the Excess Noise

In Figure 13 noise spectra are drawn for the resistor R_{43} in the device 20 at three different values of temperatures. At high frequencies the spectra approach different asymptotes due to a change in the resistivity of the layer with temperature. At low frequencies the excess noise components for the three cases are not much different (less than a factor 3). In effect there is no drastic dependence of the excess noise on temperature.

4.5 Implantation Dose Dependence of the Excess Noise

A strong dependence of the excess noise component Ieq* on the ion implantation dose appears in Figure 14. The noise spectra of R_{54} in the devices 20, 27 and 32 representing three different values of the implantation doses are plotted. It is interesting to note that there is a drastic decrease in Ieq* (more than a factor 40) for the devices implanted with 1.0 x 10^{14} B^+ ions/cm^2 as compared to the devices implanted
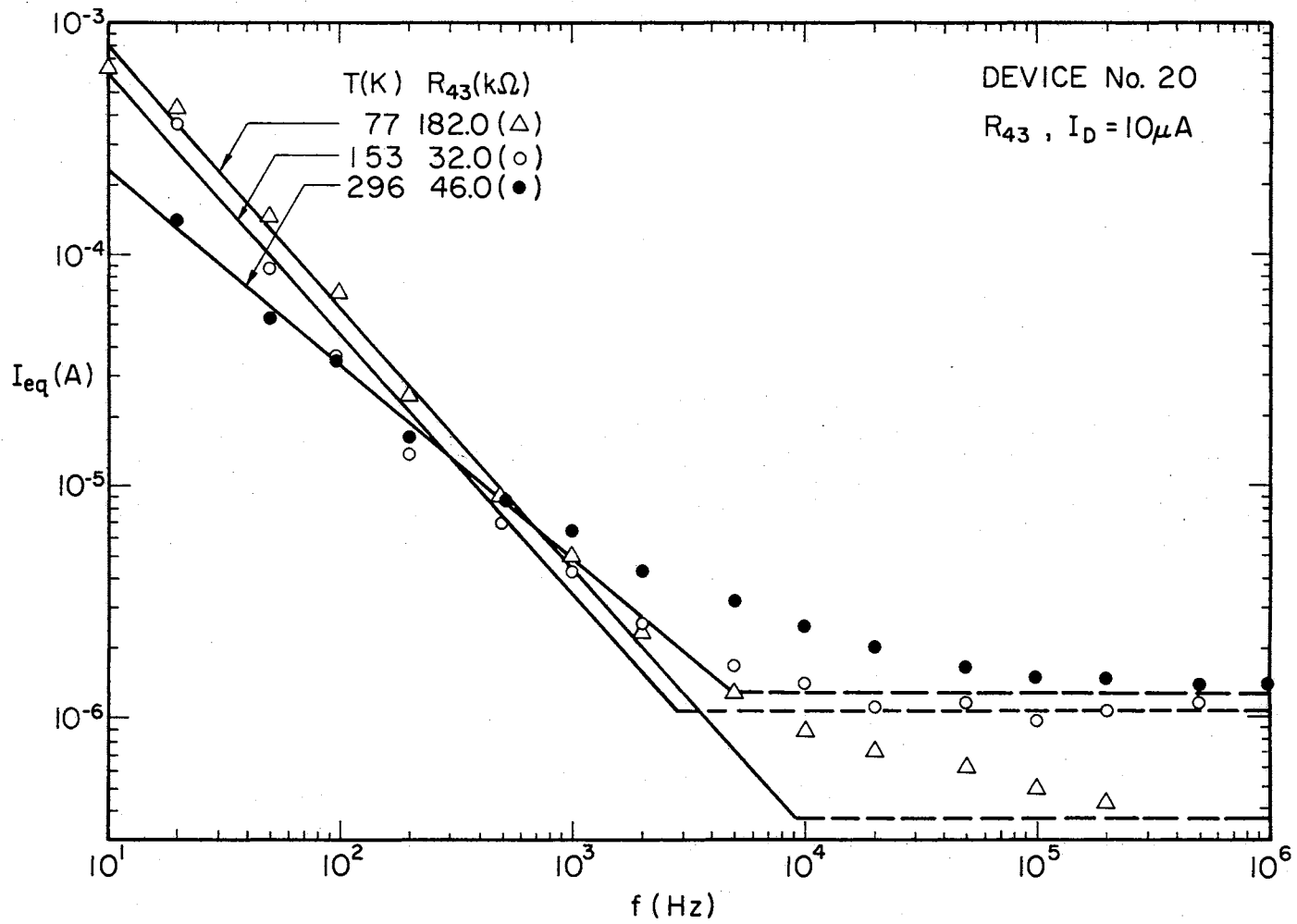
Figure 13. Noise Spectra of Resistor R_{43} in Device No. 20 for I_D = 10 μA for Three Different Temperatures
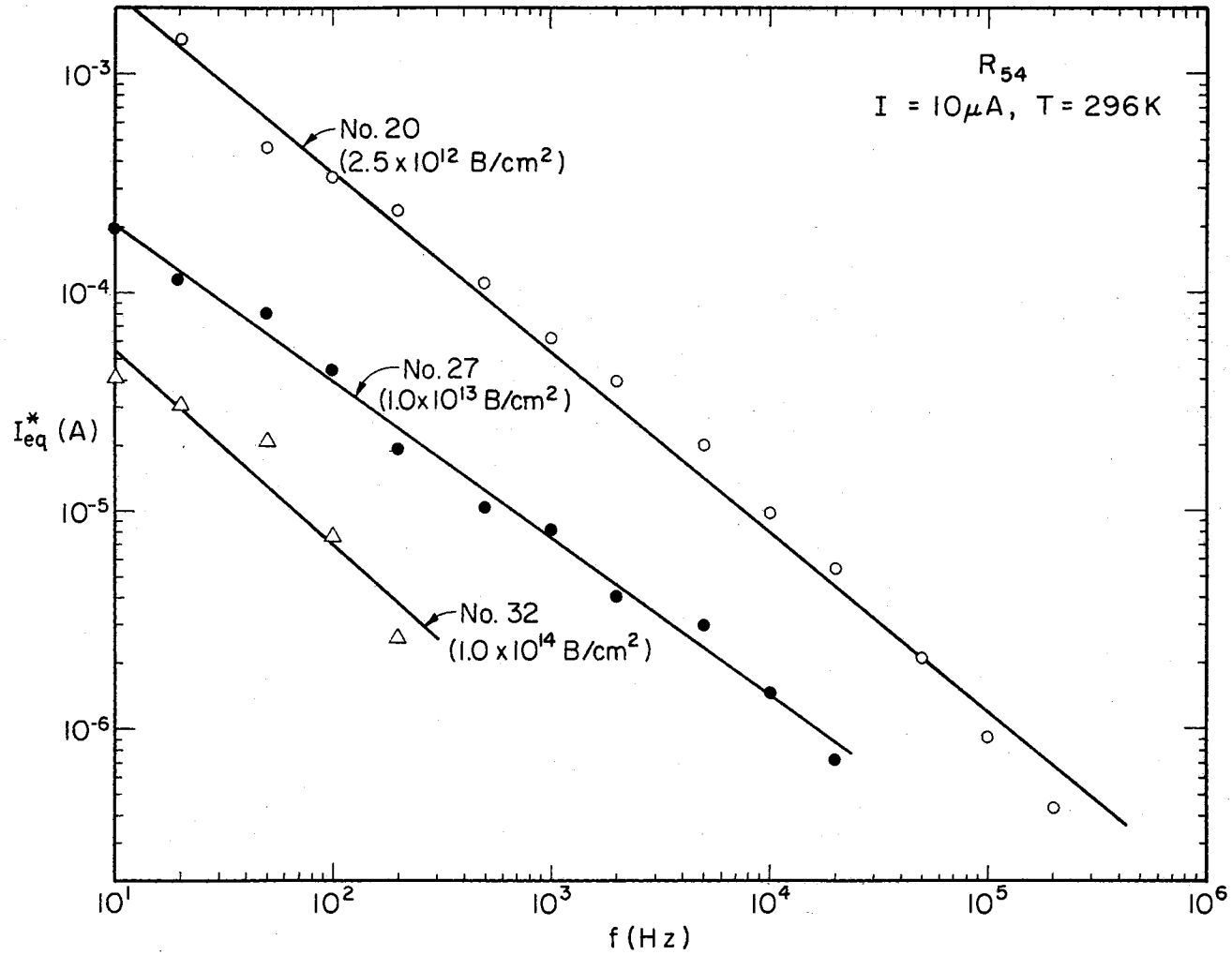
Figure 14. Noise Spectra of Resistor R_{54} in Devices 20, 27, and 32 for I_D = 10 μA

with 2.5 x 10^{12} B^+ ions/cm^2. A simple relationship between Ieq* and the implantation dose (N_I) cannot be decided from the figure. The variation of Ieq* with higher dose of implantation accounts for the noise spectra of Figure 12 where the effect of both W and N_I are felt.

4.6 Energy of Implantation Dependence of the Excess Noise

The effect of the energy of implantation on the excess noise could not be realized neatly due to nonavailability of the devices for a significant energy range. Figure 15 shows the noise spectra of the resistor R_{54} in the devices 8, 27 and 44 made with different energies of implantation but with the same dose. It is found that the noise of R_{54} in the device 8, which is made with the highest energy of implantation (= 110 keV) is the highest. Any quantitative analysis cannot be made because the variation is less than a factor 2 (corresponding to an energy variation of 110/50 = 2.2).

4.7 Effect of Substrate Bias on the Excess Noise

The noise spectra of R_{36} in the device 20 for three negative values of substrate bias are shown in Figure 16. In obtaining measurements care was taken so that pinching is brought about by the substrate bias rather than because of the voltage drop across the channel due to I_D. This was insured by using I_D such that $V_D << V_{bias}$. Larger negative substrate bias reduces the channel depth, thereby increasing the resistance values, as observed. However, the excess noise increases. A calculation shows that Ieq* $\propto R_b^2$ where R_b is the resistance of the channel for a particular value of negative substrate bias. As R_b = PL/W x D, where P is the
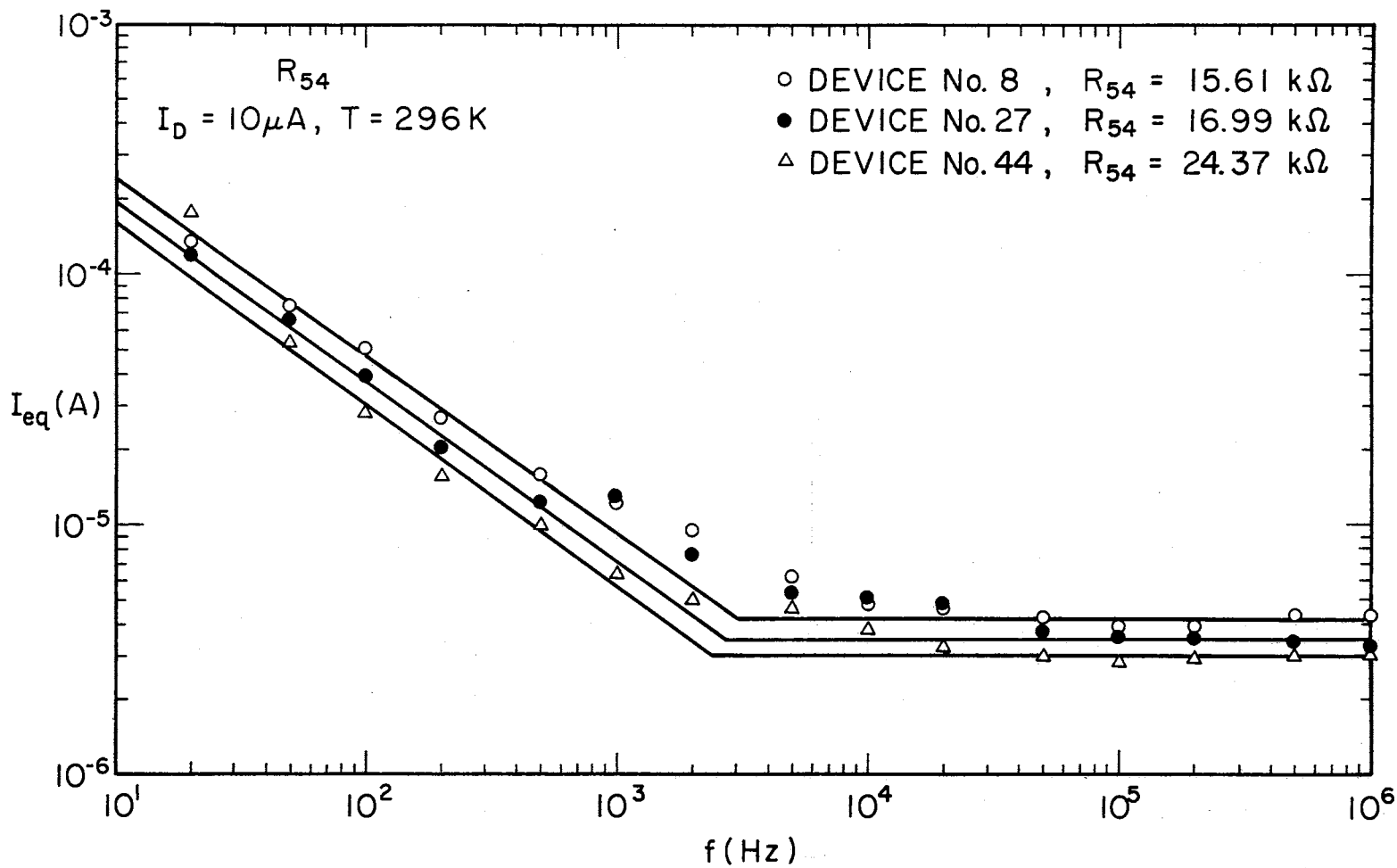
Figure 15. Noise Spectra of Resistor R_{54} in Devices 8. 27, and 44 for I_D = 10 μA
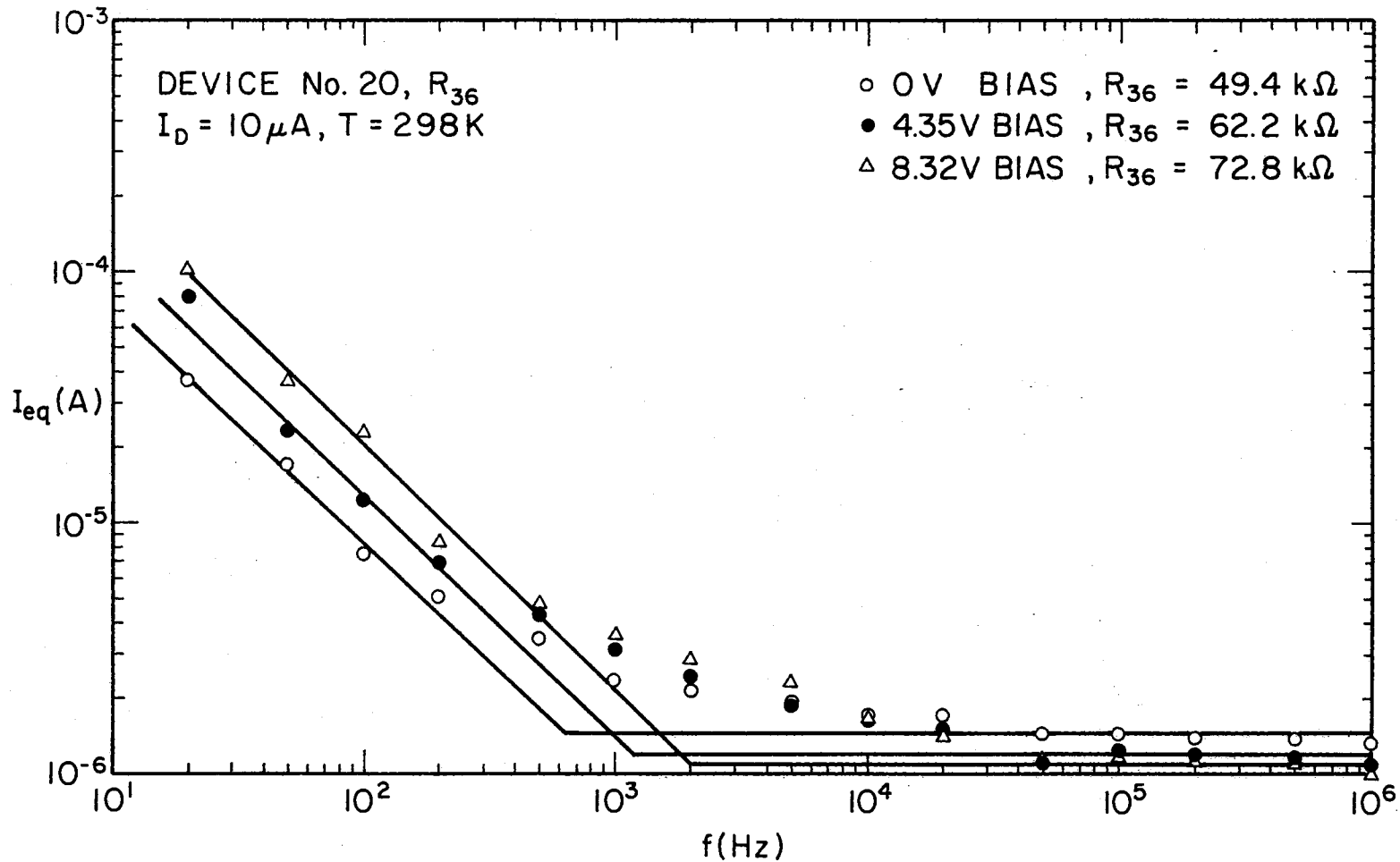
Figure 16. Noise Spectra of Resistor R_{36} in Device No. 20 for I_D = 10 µA for Three
Values of Negative Substrate Bias

resistivity (ohm · m) of the channel, and since P, L and W do not vary, $Ieq* \propto 1/D^2$.

If we combine results shown in Figures 6, 10, 11, and 16, we find

$$Ieq* \propto \left[\frac{I_D}{WD}\right]^2$$

or $Ieq* \propto j_D^2$ where j_D is the current density (A · m^{-2}) in the channel.

CHAPTER V

THEORETICAL ANALYSIS

In this chapter experimental results described in Chapter IV will be analyzed in relation to some of the existing models to explain the behavior of the excess noise.

5.1 McWhorter's Theory

McWhorter (1,3) attributes the origin of the excess noise to fluctuations in the number of trapped carriers in surface traps in a semiconductor. A time constant distribution ($1/\tau$ type) of surface traps explains $1/f$ variation of the excess noise yielding the following results for a p-type sample.

$$Si(f) = \left[\frac{qV_D}{L^2}\right]^2 [(\mu_p + \mu_n)M - \mu_{FE}]^2 Sp(f) \qquad (5.1.1)$$

and

$$Sp(f) = \frac{4 \, P_o^* S}{2\pi f \, \ln \left(\frac{\tau_2}{\tau_1}\right)} (\tan^{-1} 2\pi f\tau_2 - \tan^{-1} 2\pi f\tau_1) \qquad (5.1.2)$$

where

$Si(f)$ = excess current noise spectral density ($A^2 \cdot Hz^{-1}$);

q = electron charge (AS);

V_D = sample bias voltage (V);

L = length of the sample (m);

μ_p = hole mobility in the sample ($m^2 \cdot V^{-1} \cdot S^{-1}$);

28

μ_n = electron mobility in the sample $(m^2 \cdot V^{-1} \cdot S^{-1})$;

M = McWhorter's coefficient

$$= \frac{ALn_o}{CLP^*_o} ;$$

μ_{FE} = field effect mobility $(m^2 \cdot V^{-1} \cdot S^{-1})$;

$Sp(f)$ = spectral density of number of trapped carriers (Hz^{-1});

S = surface area of the sample (m^2);

f = frequency (Hz);

τ_1 = minimum value of time constant of surface traps (S);

τ_2 = maximum value of time constant of surface traps (S);

P^*_o = effective surface density of holes (m^{-2}) interacting with

   surface traps;

A = area of cross-section of the sample (m^2);

V = volume of the sample (m^3); and

n_o = bulk electron density in the sample (m^{-3}).

For our case of a simple geometry resistor of length L(m), width W(m), depth D(m) and bulk hole density $P_o (m^{-3})$ we have,

$$V_D = I_D R = \frac{I_D L}{q P_o \mu_p A} \qquad (5.1.3)$$

$$S = 2L(W + D) \qquad (5.1.4)$$

$$A = W \times D \qquad (5.1.5)$$

$$C = 2(W + D) \qquad (5.1.6)$$

Using Equations 5.1.3, 5.1.4 and 5.1.5, and combining Equations 5.1.1 and 5.1.2 we deduce,

$$Si(f) = \frac{4\ P^*_o\ I_D^2}{\pi f\ P_o^2\ \ell n\ (\frac{\tau_2}{\tau_1})} \times \frac{1}{L} \times \frac{(W + D)}{(W \times D)^2}$$

$$\times \left[(1 + \frac{\mu_n}{\mu_p}) \times \frac{WDn_o}{2P^*_o(W + D)} - \frac{\mu_{FE}}{\mu_p}\right]^2 \times (\tan^{-1} 2\pi f\tau_2 - \tan^{-1} 2\pi f\tau_1)$$

$$(5.1.7)$$

or in our notation

$$Ieq^* = \frac{1}{2q}\ Si(f)$$

$$= \frac{2\ P^*_o\ I_D^2}{\pi\ q\ f\ P_o^2\ \ell n\ (\frac{\tau_2}{\tau_1})} \times \frac{1}{L} \times \frac{W + D}{(W \times D)^2}$$

$$\times \left[(1 + \frac{\mu_n}{\mu_p}) \times \frac{WDn_o}{2P^*_o(W + D)} - \frac{\mu_{FE}}{\mu_p}\right]^2 \times (\tan^{-1} 2\pi f\tau_2 - \tan^{-1} 2\pi f\tau_1)\ .$$

$$(5.1.8)$$

McWhorter's theory as represented by Equation 5.1.8 does not predict the proportionality of Ieq* to j_D^2 and is, therefore, inconsistent with our results. Also, the dependence on L is stronger than what our measurements show.

5.2 Hooge's Model

Hooge (7,8,9) suggests an empirical model as a result of his measurements to explain the excess noise in homogeneous samples. According to him the excess noise can be expressed as

$$\overline{(\frac{\Delta R}{R})^2} = C\ \frac{\Delta f}{f}$$

$$(5.2.1)$$

where ΔR is the fluctuation in the resistance R of a sample, Δf is the bandwidth of measurement, f the frequency and C a constant. An

estimation of C can be made as follows:

$$C = \frac{\alpha}{N_{total}} \qquad (5.2.2)$$

where α is an experimentally found dimensionless constant and N_{total} is

the total number of mobile charge carriers in the sample.

If we associate a corresponding fluctuation ΔI in current and ΔV in

voltage to ΔR we have

$$\overline{(\frac{\Delta R}{R})^2} = \overline{(\frac{\Delta V}{V})^2} = \overline{(\frac{\Delta I}{I})^2} = C\frac{\Delta f}{f} \qquad (5.2.3)$$

or in our notation,

$$Ieq^* = \frac{I_D^2}{2q} \cdot C \cdot \frac{1}{f} \qquad . \qquad (5.2.4)$$

Writing C as $C = \frac{\alpha}{\varepsilon N_I \times W \times L}$ (Equation 5.2.2), where N_I is the

implantation dose and ε is the annealed fraction of the implanted layer,

we have from Equation 5.2.4,

$$Ieq^* = \frac{I_D^2}{2q} \cdot \frac{\alpha}{\varepsilon N_I \times W \times L} \cdot \frac{1}{f} \qquad . \qquad (5.2.5)$$

In the above equation, representing Hooge's model, Ieq* dependence

on j_D^2 is again missing. Also the dependence on L and N_I is not in

accordance with our measurements.

5.3 Müller's Theory

Müller (4,5,6) suggests a thermal feedback theory for the possible

origin of the excess noise in diodes and transistors. Consider that a

noise current pulse, Δi, occurs in a differential volume element dV in a

p-n junction. This current pulse, having a shot and thermal noise com-

ponent, flows across the potential V across the junction and a noise

power pulse, ΔP, and therefore a heat pulse is generated. The low-frequency components of the spectrum of this pulse are not short circuited by the thermal capacitances surrounding the volume element dV and therefore produce a local temperature change ΔT in dV. The transfer function relating these two quantities (ΔP and ΔT) is the complex thermal impedance Z_t between the volume element dV and the ambient. It can be represented by cascading an infinite number of parallel $R_t C_t$ networks where R_t, C_t and τ are thermal resistances, capacitances and time constants, respectively. The strong temperature dependence of the current flowing through the p-n junction now generates an additional current pulse Δi_f which produces the excess noise.

In (6) Müller has used the above concept of thermal feedback to calculate the excess noise in p-n junctions arising due to high values of shot noise current in the microscopic domain considering the diode junction to be made up of a large number of "subdiodes". He specifies that the source of the excess noise is located in the depletion layer of a p-n junction. It should be pointed out, in relation of our measurements, that our devices were simple resistors with no shot noise since there were no junctions involved. Thus it seems that the mechanism that explains the origin of the excess noise is more general. In other words any theory which is developed to explain the excess noise behavior should not only account for the excess noise in devices that possess shot noise but also devices that do not show shot noise.

CHAPTER VI

CONCLUSIONS

Our measurements indicate the following about the excess noise of boron implanted layers in silicon - (a) the excess noise is directly proportional to (current density)^2 in the layer; (b) the excess noise does not depend much on the length of the layer; (c) the excess noise has a weak dependence on the temperature; (d) the excess noise has a strong inverse dependence on the implantation dose; and (e) the excess noise depends directly, rather weakly, on the energy of implantation.

Various theories about excess noise appear to be incomplete. It is speculated by the author that excess noise seems to be as fundamental in origin as Nyquist noise or shot noise. Proportionality to (current density)^2 suggests that a model which incorporates "volume effect" is more acceptable. The notion of attributing the origin of excess noise to "surface effects" does not seem to be correct.

6.1 Recommendations for Further Study

This thesis provides experimental information about the excess noise. It would be interesting to take up a study that interprets this information and suggests a theory which is complete in explaining the nature and origin of the excess noise. Further experimentation using different devices should also be worthwhile.

BIBLIOGRAPHY

(1) Van der Ziel, A. Fluctuation Phenomena in Semiconductors. London:
        Butterworths Scientific Publications, 1959, Chapter 5.

(2) Hawkins, R. J., I. R. M. Mansour, and G. G. Bloodworth. "Current
        Noise in M.O.S. Transistors at Very Low Frequencies." Confer-
        ence on Physical Aspects of Noise in Electronics Devices,
        Sept. 11-13, 1968, University of Nottingham. Peter Peregrinus
        Ltd., 127.

(3) McWhorter, A. L. "1/f Noise and Germanium Surface Properties."
        Semiconductor Surface Physics. Ed. R. H. Kingston.
        Philadelphia: University of Pennsylvannia Press, 1957, 207.

(4) Müller, O. and J. Pest. "Thermal Feedback in Power Semiconductor
        Devices." IEEE Trans. on Electron Devices, ED-17, No. 9
        (Sept., 1970), 770.

(5) Müller, O. "Thermal Feedback: A Cause for 1/f Flicker Noise in
        Transistors." International Symposium on Noise of Active
        Semiconductor Components, Sept., 1971, Toulouse, France.

(6) Müller, O. "Flicker Noise in P-N Junctions." Symposium on Noise in
        Electronic Materials and Devices, Dec. 11-12, 1972, University
        of Florida, Gainsville, Florida.

(7) Hoppenbrouwers, A. M. H. and F. N. Hooge. "1/f Noise of Spreading
        Resistances." Philips Research Reports, 25 (1970), 69-80.

(8) Hooge, F. N., H. J. A. Van dijk, and A. M. H. Hoppenbrouwers. "1/f
        Noise in Epitaxial Silicon." Philips Research Reports, 25
        (1970), 81-86.

(9) Hooge, F. N. Physics Letters, 29A (1969), 139-140.

(10) Diamond, L. and A. Siefert. "Designing Differential FET Inputs With
        Overall Performance in Mind." Electronics, 44, No. 13 (June
        21, 1971), 76-80.

(11) Van der Ziel, A. Fluctuation Phenomena in Semiconductors. London:
        Butterworths Scientific Publications, 1959, Chapter 2.

(12) Mayer, J. W., L. Erikson, and J. A. Davies. _Ion Implantation in Semiconductors_. New York: Academic Press, 1970, Chapters 1 and 2.

(13) Van der Ziel, A. _Noise: Sources, Characterization, Measurement_. New Jersey: Prentice Hall Inc., 1970, p. 174.

APPENDIX A

ION IMPLANTATION PROCEDURE

Ion implantation (12) is a method of introducing atoms into the sur-
face layer of a solid substrate by bombardment of the solid with ions in
the keV to MeV energy range. This provides an alternative mechanism of
introducing dopant atoms into the lattice. The procedure involves
impinging a beam of dopant ions acclerated through a potential of
10 - 100 kV on the semiconductor surface.

Doping by implantation provides potential advantages over conven-
tional evaporation and diffusion techniques. It is important to note
that in this process the number of implanted ions is controlled by the
external system rather than by physical properties of the substrate which
is typical of the diffusion process. In thermal diffusion, surface con-
centration and dopant profile are related to the solubility of dopant
species in the substrate species and also on the process temperature. In
ion implantation, on the other hand, these two quantities are independ-
ently controlled - the profile of implanted ions is a function of the
accelerating voltage and the number of implanted ions is determined by
the integrated ion beam current.

Because of the advantages of the ion implantation procedure illus-
trated above together with the ability to focus and align the ion beam
accurately, devices with very little uncertainty in geometry and carrier
concentration can be produced.

APPENDIX B

DEVICES LAYOUT

The devices used were simple ion implanted resistors. Figure 17 shows the lengthwise and sidewise sections of a typical resistor. For all the devices the substrate used was an n-type silicon of resistivity of 3 ohm · cm. Ion implantation was done using a mask with boron ions with different values of implantation doses and energies resulting in a matrix of devices shown in Figure 18. The layers were then partially annealed at 545° C and finally passivated with a very thin layer of silicon dioxide. A picture of various resistors available in each device and nomenclature of contacts is shown to scale in Figure 19. All contacts numbered were made with heavy boron diffusion. The picture represents a top view imagining implantation is done into the paper.

I - RESISTOR
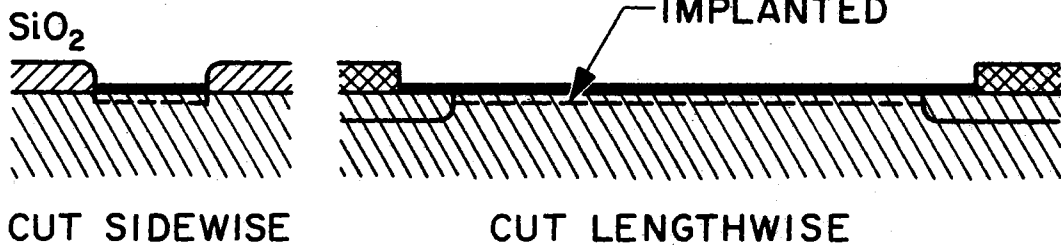
Figure 17. Sectional View of a Typical Implanted Resistor

IMPLANTATION DOSE B IONS/CM^2	IMPLANTATION ENERGY (k ev)		
	50	80	110
2.5×10^{12}	39, 40, 41	20, 22, 23	1, 2, 3
1.0×10^{13}	44, 45, 46	27, 28, 29	8, 9, 10
1.0×10^{14}	50, 51, 52	32, 33, 34	16, 17, 18

Note: Numbers inside squares indicate device numbers

Figure 18.   Nomenclature of Devices

Figure 19.   Nomenclature of Contacts and Relative Dimensions of Resistors
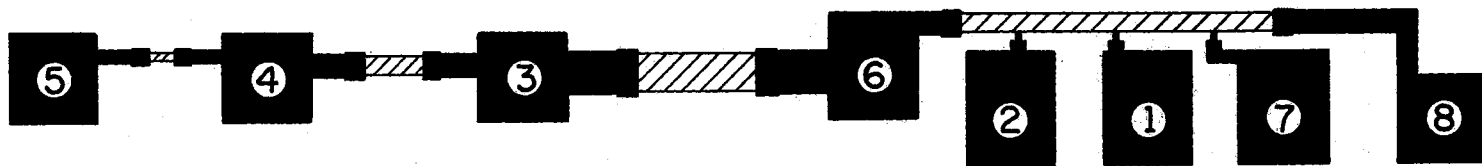
APPENDIX C

MEASUREMENT EQUIPMENT LAYOUT

C.1 The Apparatus

A block diagram of experimental layout to measure the excess noise is shown in Figure 20. This specialized equipment referred to as noise analyzer was made available through integrated research efforts both at Oklahoma State University and California Institute of Technology.

The wave analyzer was used to detect the RMS value of noise voltage at a particular tuned frequency in a specific bandwidth. The integrator integrated proportionally the output of the wave analyzer to take an average of the fluctuating RMS voltage over a time period adjustable between 1 and 100 seconds. The output of the integrator was displayed on a digital voltmeter and was recorded. The oscilloscope was used to monitor the output of the preamplifier so that any spurious signals could be detected.

It follows (13) that the statistical error $\Delta\overline{V}$ in the measurement of an average $\overline{V}$ of a fluctuating voltage is given by

$$\frac{\Delta\overline{V}}{\overline{V}} = \frac{1}{\sqrt{2 \cdot \Delta f \cdot T}} \qquad (C.1.1)$$

where Δf is the bandwidth of the measuring instrument and T is the time period over which the average is taken. Since the bandwidth Δf was fixed, being 6 Hz for wave analyzer HP302A, for measurements below 50 kHz an averaging (integration) time of 20 seconds was used to make a good
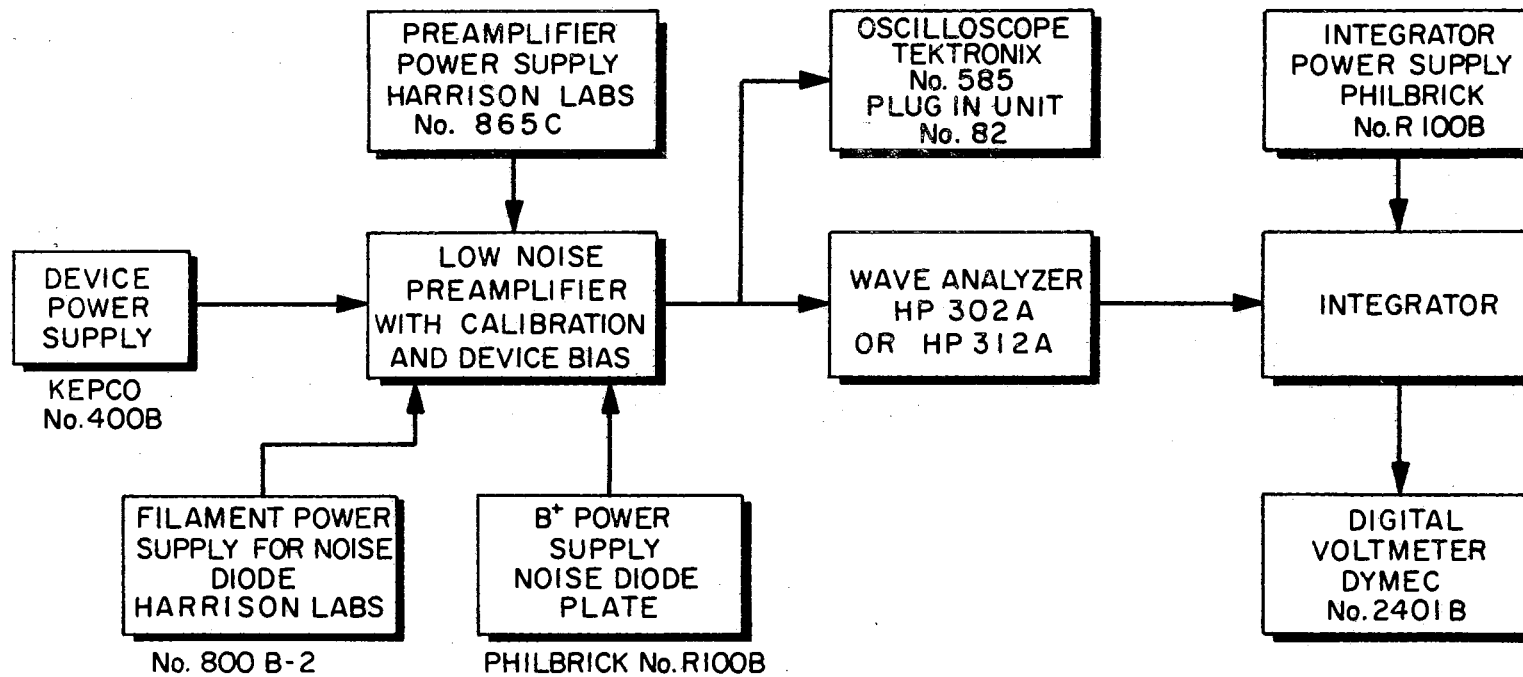
41

Figure 20. Block Diagram of Experimental Layout for Noise Measurement

compromise between errors and speed for collecting data. For high frequency measurements above 100 kHz wave analyzer HP312A with bandwidth 3 kHz and integration time of 5 seconds was employed. At each tuned frequency three measurements were recorded and then an average taken.

In our notation of measured quantities

$$Ieq = \frac{\overline{V_1^2} - \overline{V_S^2}}{\overline{V_2^2} - \overline{V_1^2}} \cdot I_C \tag{C.1.2}$$

where

$\overline{V_1^2}$ = mean square voltage measured by the digital voltmeter when the input terminals of the preamplifier are open and there is no current through the noise diode;

$\overline{V_S^2}$ = mean square voltage measured by the digital voltmeter when the input terminals of the preamplifier are shorted; and

$\overline{V_2^2}$ = mean square voltage measured by the digital voltmeter when the input terminals of the preamplifier are open and a calibration current I_C is passed through the noise diode.

C.2 Equipment Checking and Calibration

Before taking any kind of measurements the accuracy of various units of the noise analyzer was checked and calibration was done plotting thermal noise spectra of metal film resistors of known value and comparing with the calculated values. Steps involved can be grouped into three categories.

C.2.1 <u>Measuring Instruments Accuracy Check</u>

The standard used to check the accuracy of all meters used was the

Dymec 2401B Integrating Digital Voltmeter which has a specified accuracy

of $\pm$ 0.01%. It was assumed that this instrument was still within the

specified accuracy limits.

Triplett type 630NA was used to measure device current I_D. It has a

specified accuracy of $\pm$ 1.5%. Its accuracy was checked by passing a

known current (as read by the triplett) through a known resistance

(50 K $\pm$ 1%) and monitoring the voltage drop on the Dymec. The meter was

found to be within the specified accuracy limits.

The noise tube calibration current (I_C) meter was checked using the

triplett. Its reading was found to be very close (< 3%) to the reading

of the triplett.

C.2.2 <u>Linearity Checks</u>

The integrator's linearity was checked by applying a known DC

voltage to its input and recording its output (both measurements were

taken with the Dymec). A plot of input-output voltage characteristics of

the integrator for input voltage range 0.1 to 1 V (1 volt is the maximum

output from the wave analyzer) is shown in Figure 21. It was found that

for both time periods of integration of 5 seconds and 20 seconds the

integrator was strictly linear.

To check the linearity of the preamplifier a resistor R_{26} (6.3 kΩ)

in device no. 32 was randomly chosen and a current 50 µA was flown

through it. A plot was made between $\overline{V_2^2}$ and I_C (the calibration noise

diode current) at a low value of frequency equal to 40 Hz. This is shown

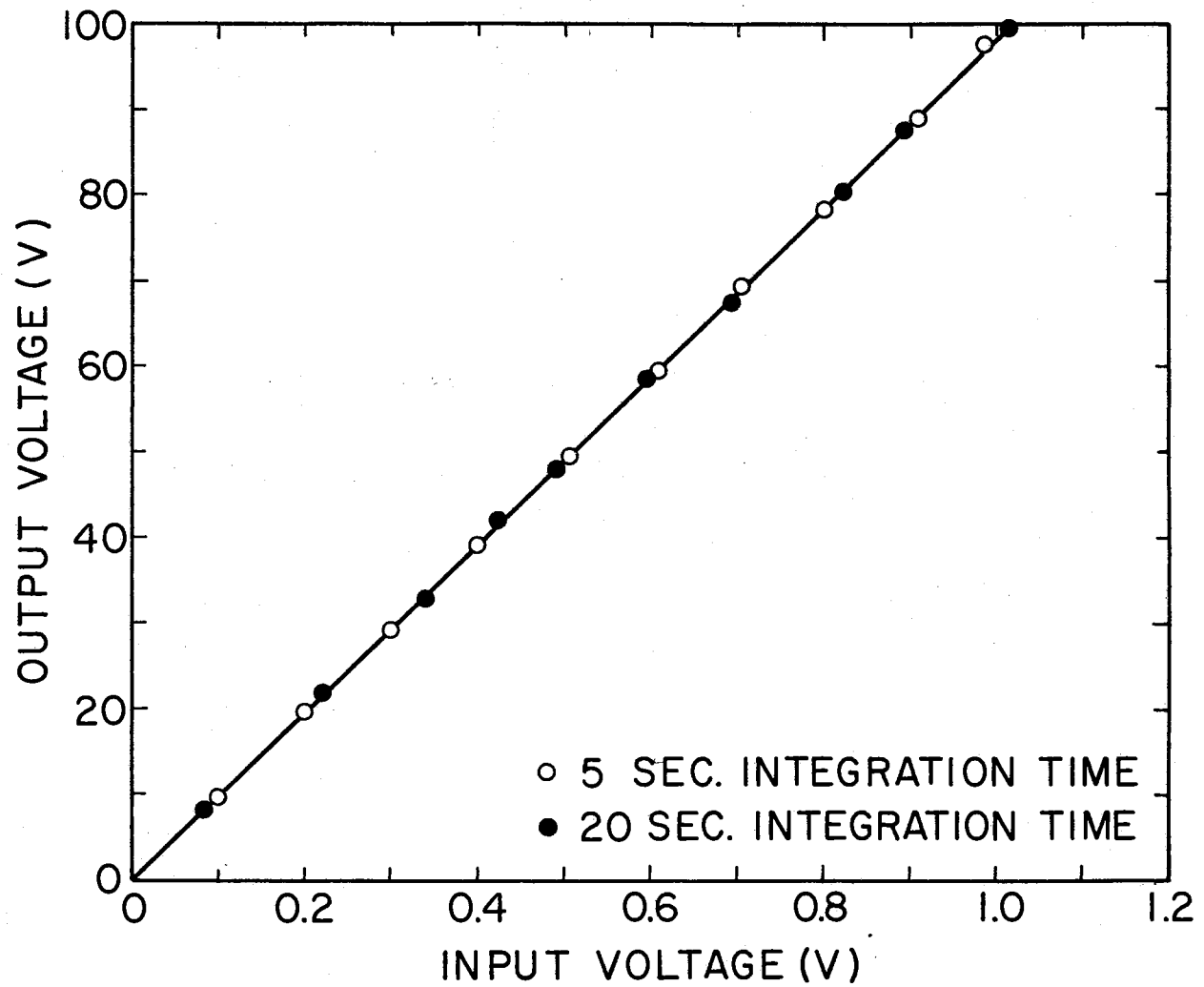in Figure 22. The linearity of the plot assured the linearity of the

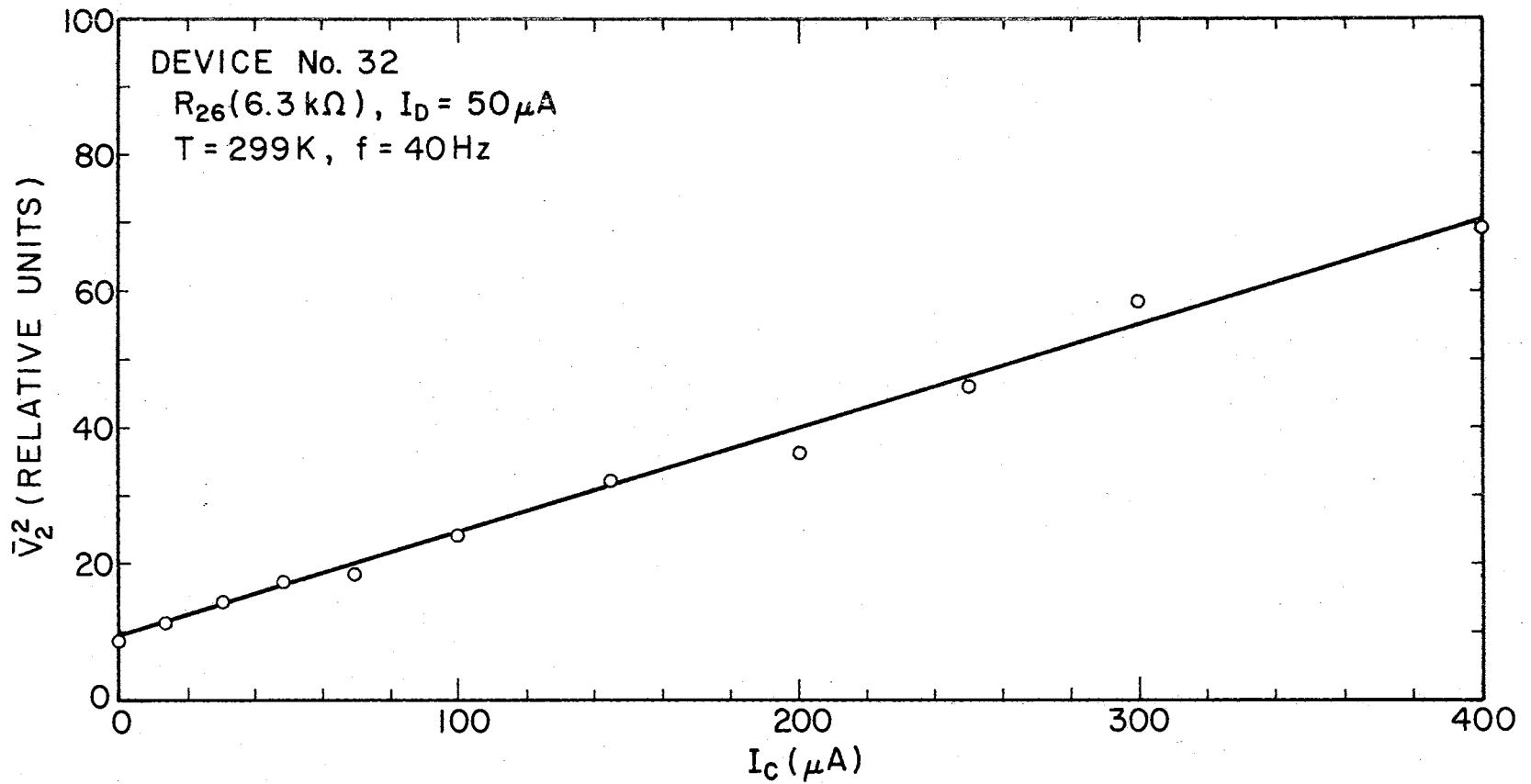Figure 21: Input-Output Characteristics of the Integrator

Figure 22. $\overline{V_2^2}$ vs. I_C for Resistor R_{26} in Device No. 32 for I_D = 50 µA at f = 40 Hz

preamplifier in agreement with Equation C.1.2.

C.2.3 Calibration With Metal Film Resistors

Figure 23 shows a comparison between measured noise spectra and theoretical calculated Ieq(= $\frac{2}{q}\frac{kT}{R}$) for two resistors (R), 10.6 kΩ and 500 kΩ. In case of measuring noise spectra of 500 kΩ a DC current equal to 100 μA was flown through it. In both cases the average measured value of Ieq differs by less than 10% from the calculated value.
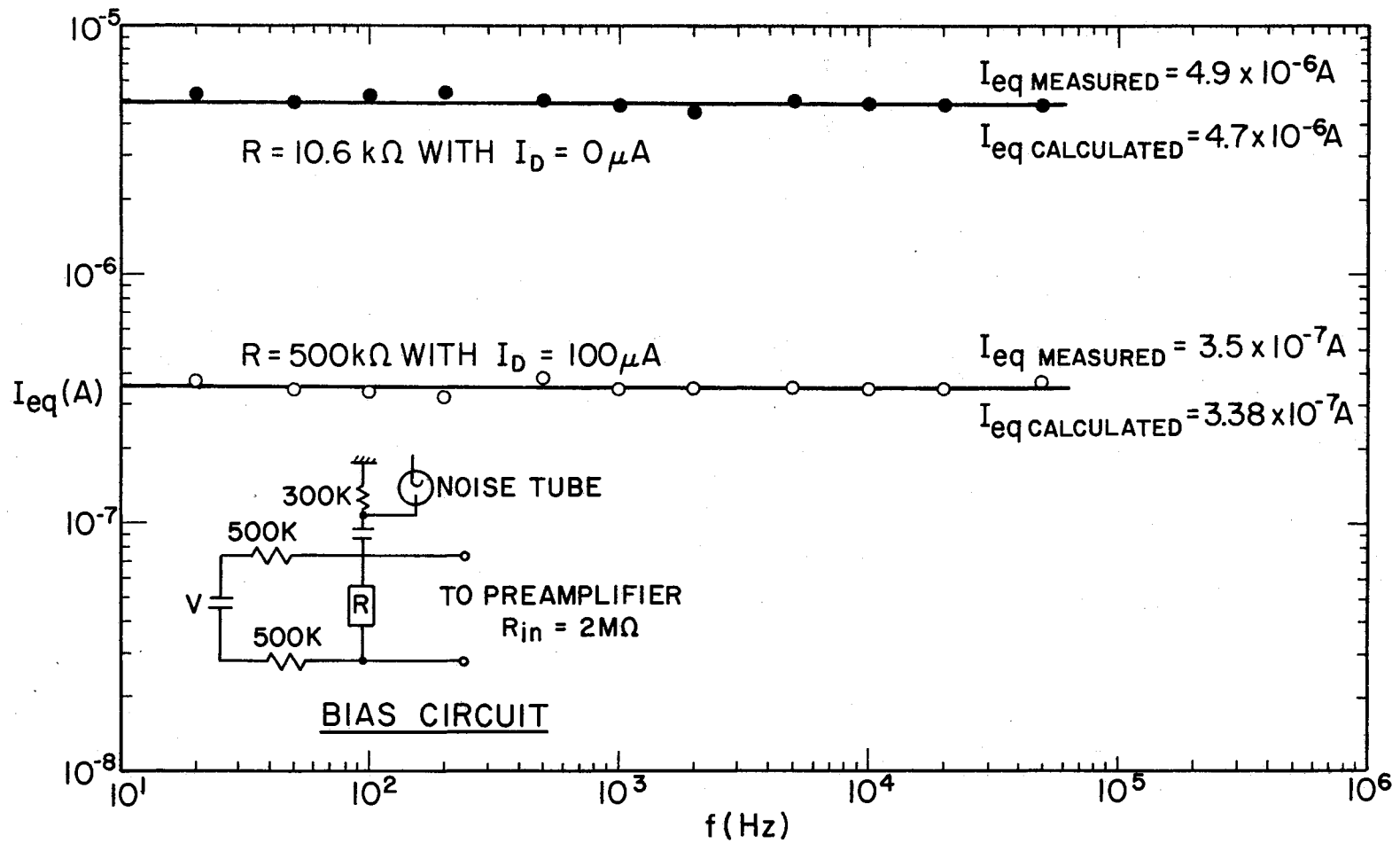
Figure 23. Noise Spectra of Two Resistors: 10.6 kΩ With I_D = 0 and 500 kΩ With I_D ≐ 100 μA

VITA

Jawahar Lal Tandon

Candidate for the Degree of

Master of Science

Thesis: EXCESS NOISE SPECTRAL ANALYSIS OF BORON IMPLANTED LAYERS IN
          SILICON

Major Field: Electrical Engineering

Biographical:

Personal Data: Born on September 19, 1949, in Agra, India, the son
     of Mr. and Mrs. A. P. Tandon.

Education: Attended primary and secondary schools in New Delhi,
     India, and graduated from Air Force Central School, New Delhi,
     India in September, 1965; received the Bachelor of Technology
     degree in Electrical Engineering from the Indian Institute of
     Technology, Kanpur, India, in October, 1970; completed require-
     ments for Master of Science degree at Oklahoma State University
     in May, 1973.

Professional Experience: Employed by the School of Electrical
     Engineering of Oklahoma State University as a Graduate
     Assistant from January, 1972 to May, 1973.

Professional Organizations: Member of Eta Kappa Nu.